Single-shot electron diffraction using a cold atom electron source

IOP Publishing Journal of Physics B: Atomic, Molecular and Optical Physics
J. Phys. B: At. Mol. Opt. Phys. **48** (2015) 214002 (6pp) doi:10.1088/0953-4075/48/21/214002

Single-shot electron diffraction using a cold atom electron source

Rory W Speirs[1], Corey T Putkunz[1], Andrew J McCulloch[1], Keith A Nugent[2], Benjamin M Sparkes[1] and Robert E Scholten[1]

[1] School of Physics, The University of Melbourne, Victoria, 3010, Australia
[2] ARC Centre of Excellence for Advanced Molecular Imaging, Department of Physics, La Trobe University, Victoria 3086, Australia

E-mail: scholten@unimelb.edu.au

Received 4 June 2015, revised 30 July 2015
Accepted for publication 7 August 2015
Published 23 September 2015

Abstract

Cold atom electron sources (CAESs) are a promising alternative to traditional photocathode sources for use in ultrafast electron diffraction due to greatly reduced electron temperature at creation, and the potential for a corresponding increase in brightness. Here we demonstrate single-shot, nanosecond electron diffraction from monocrystalline gold using cold electron bunches generated in a CAES. The diffraction patterns have sufficient signal to allow registration of multiple single-shot images, generating an averaged image with significantly higher signal-to-noise ratio than obtained with unregistered averaging. Reflection high-energy electron diffraction was also demonstrated, showing that CAESs may be useful in resolving nanosecond dynamics of nanometre scale near-surface structures.

Keywords: cold atom electron source, ultrafast electron diffraction, diffraction imaging

(Some figures may appear in colour only in the online journal)

1. Introduction

Ultrafast single-shot diffraction is revolutionizing our understanding of materials science, chemistry, and biology, by imaging objects on atomic length and time scales simultaneously [1–3]. X-ray free electron lasers (XFELs) have been used to perform single-shot coherent diffractive imaging on micro- and nano-metre scale targets [4, 5], where the imaging pulse is briefer than the time scale of damage to the object [6, 7]. An alternative and complementary approach is ultrafast electron diffraction, which benefits not only from much stronger scattering of electrons relative to x-rays [8], but also significantly reduced damage per elastic scattering event [9]. To enable single-shot diffraction studies, the number of electrons per pulse must be of order 10^6 or greater to have sufficient signal per pixel at the detector [10]. This number is easily achievable with photocathode sources, and when combined with RF bunch compression, sub 100 fs pulses have been achieved [11]. The brightness of photocathode sources is limited by the high initial temperature of the extracted electrons (10^4 K), leading to a high transverse emittance [12]. The emittance required for single-shot imaging depends on the size of the object being imaged: larger object sizes or crystal periods require lower emittance to generate useful coherent diffraction patterns. Ultrafast single-shot electron diffraction has been achieved from large single crystal and polycrystalline samples using a variety of photocathode based sources [13–17], but insufficient source brightness has prevented demonstration for micro or nanocrystals, or single molecules.

Cold electron sources are a promising alternative to solid state photocathodes, producing electrons by near threshold photoionization of laser cooled atoms. Electrons from these sources have an intrinsic temperature as low as 10 K, which for a given flux leads to several orders of magnitude increase in brightness [18, 19]. The low electron temperature, together with the ability to spatially shape the beam [20], should allow these sources to produce uniformly filled ellipsoid bunches, which do not suffer emittance degradation resulting from nonlinear internal Coulomb forces [21].

A cold electron source was recently used for the first time to generate a transmission electron diffraction pattern [22]. In that experiment, cold, sub-picosecond electron pulses containing a few hundred electrons were scattered by graphite. To

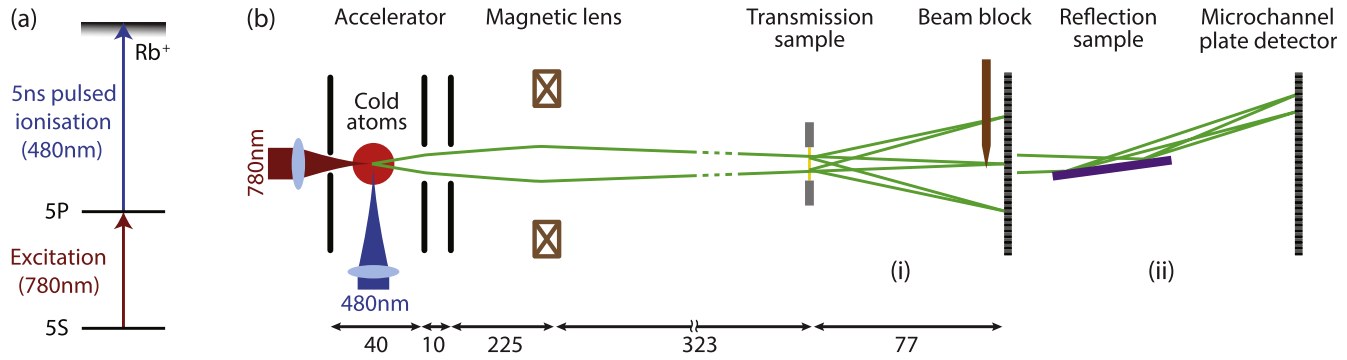

Figure 1. (a) Rubidium atoms are ionized in a two step process: 780 nm laser light drives them to the first excited state where they are ionized by a 5 ns pulse of 480 nm light. (b) The electrons produced are accelerated by a static electric field, focused, and scattered off a sample, either in transmission (i) or reflection (ii) geometries. Distances are in millimetres.

produce diffraction patterns with clearly discernible Bragg reflections, several thousand individual shots were integrated.

Here we present the first *single-shot* electron diffraction patterns obtained using a cold electron source. The patterns were obtained from a monocrystalline gold foil using a single 5 ns bunch of 5×10^5 electrons. No electron aperture was required due to the high spatial coherence of the electrons at the source. This allowed all generated electrons to contribute to the image, resulting in a single shot with sufficiently high signal-to-noise ratio for identification of the sample and registration of successive images. Single-shot reflection high-energy electron diffraction (RHEED) was also demonstrated from a wafer of monocrystalline silicon.

2. The cold atom electron source (CAES)

The CAES generates electrons by photoionization of rubidium-85 atoms in a magneto-optical trap, which is positioned between two accelerating electrodes as shown in figure 1(b).

The photoionization is a two-stage process (figure 1(a)). The atoms are excited from the $5S_{1/2}(F = 3)$ ground state to the $5P_{3/2}(F = 4)$ excited state using a 100 ns pulse of laser light of wavelength 780 nm. A 5 ns pulse from the ionization laser (wavelength 480 nm) then drives the atoms either to a Rydberg level, or directly to the continuum.

The excitation laser illuminates the atom cloud along the axis of electron propagation (longitudinal direction), and the focused intensity profile can be changed arbitrarily using a liquid crystal spatial light modulator, which defines the shape of the electron bunch in the two dimensions transverse to propagation [20]. The blue ionization laser illuminates the atom cloud transversely to the electron propagation axis, defining the longitudinal profile of the electron bunch which is generated in the region of overlap of the two laser beams such that the bunch is shaped in all three-dimensions.

The ionization time is determined by the temporal profile of the blue tunable dye laser pulse, with full width half maximum (FWHM) duration of 5 ns, pulse energy of 5 mJ at the cloud, and repetition rate of 10 Hz. The blue laser is focused with a cylindrical lens onto the atom cloud, so that the ionization region is defined by a ribbon of light with a FWHM width of 30 μm in the longitudinal direction.

Before ionization the atom cloud has a peak density of 10^{10} atoms cm^{-3} and temperature 100 μK. The quadrupole magnetic field is switched off and allowed to decay for 3.5 ms before ionization, but a remnant magnetic field alters the electron trajectory slightly from shot to shot.

The accelerator can be used in a two or three electrode configuration. The arrangement of applied potentials allows flexibility in determining the extraction electric field strength, the final energy of the electrons, and the diverging beam angle, which is defined in part by the lensing effect of the electrodes. In addition, the energy spread of the extracted electrons is determined by the combination of extraction electric field strength and longitudinal width of the ionization region. A standard configuration of potentials with field strength 2.6 kVcm^{-1} and a blue beam width of 30 μm results in an electron energy spread of 8 eV. This is a relatively high energy spread compared to sources used in conventional electron microscopes, where chromatic aberration in the strong objective lens drives the need for low energy dispersion. The contribution to the point spread function due to chromatic aberration is proportional to the beam semi-angle accepted into the lens, and for the single weak condenser lens used in our setup, this contribution is significantly smaller than the detector resolution. Polychromaticity also results in a spread of diffraction angles for any given sample spatial frequency, limiting the achievable resolution in coherent diffractive imaging. We typically use an electron energy of 8 keV for diffraction experiments, giving a fractional energy spread of $\Delta E/E < 0.001$, which contributes negligibly to the spread in diffraction angles from the sample, and would allow coherent diffractive imaging of 20 nm objects to a resolution of better than 1 Å [23]. The energy spread could be reduced further if required by tailoring the extraction field strength or reducing the focal spot size of the blue laser beam, though the latter would also reduce the number of electrons generated.

After the electron bunch leaves the accelerator, it traverses a solenoid magnetic lens at a distance of 225 mm, before drifting 323 mm to the sample. The low numerical aperture of the lens limits the ability to create very small beam sizes at the sample, but results in a highly collimated beam

without the need to introduce further electron optics. After the target sample the diffracted electrons propagate 77 mm to a phosphor-coupled microchannel plate (MCP) detector which is imaged with a camera.

3. Beam parameters

We used a Gaussian excitation laser beam of width 80 μm FWHM at the focus, with peak intensity thousands of times the saturation intensity to maximize the bunch charge. The effective excitation volume was increased by saturation broadening and reabsorption of radiative decay. The effective width of the source was 1.4 mm FWHM, determined from the unfocused electron bunch size at the detector and the known magnification of the electron optics. The source divergence of our source is $\sigma_{\theta_x} = 0.3$ μrad [18], giving a source emittance of $\epsilon_x = 50$ nm rad. The electrons were focused to a minimum spot size at the MCP as shown in figure 1, with beam width at the sample of approximately 300 μm, and corresponding coherence length at this point of $\ell_c = 2$ nm. Using a Faraday cup, the number of electrons per pulse was measured as 5×10^5 (80 fC), corresponding to an ionization fraction of approximately 50% within the ionization region. The bunch temporal profile was estimated to be Gaussian with a duration of 5 ns FWHM based on the shape of the blue laser pulse, leading to a peak beam current of 20 μA and peak brightness of $\mathscr{B} = 3 \times 10^8$ A m^{-2} sr^{-1} [18].

The emittance and bunch charge for the CAES are therefore approaching the values required for single-shot diffraction of microcrystals [24], but the pulse duration is up to six orders of magnitude too long to avoid degradation of the diffraction pattern due to beam induced damage of such small samples. Recent studies have suggested the constraints on pulse duration due to damage could be relaxed for electrons compared with x-rays, because of the differences between the scattering and damage-inducing processes [25]. To achieve sub-picosecond ultrafast electron diffraction, the ionization process can be modified to use femtosecond rather than nanosecond laser pulses [18, 19]. Picosecond to femtosecond duration electron bunches containing the same charge will require spatial beam shaping in order to avoid brightness degradation caused by the otherwise nonlinear space charge expansion of the bunch [26].

4. Single-shot electron diffraction

We demonstrated diffraction of electron bunches generated in the CAES from an 11 nm thick gold foil mounted on a 3 mm transmission electron microscopy grid, with an electron energy of 8 keV. Figure 2 shows the diffraction pattern from a single 5 ns electron bunch. The resulting Bragg reflections are clearly visible out to the $(\overline{2}\overline{4}0)$ spot at a resolution of 1.1 Å^{-1}, where the crystallographic convention has been adopted for reciprocal lattice vectors, such that $|\mathbf{g}_{hkl}| = 1/d_{hkl}$, where d_{hkl} is distance between atomic planes in real space.

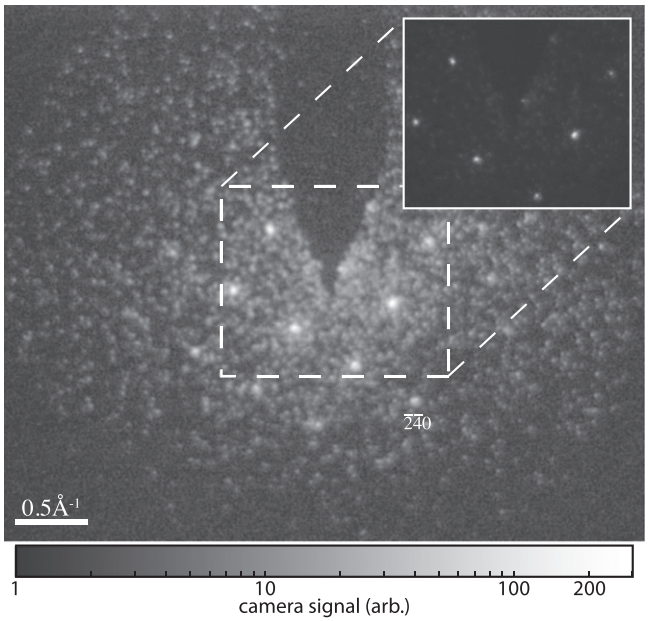

Figure 2. Single-shot transmission electron diffraction from gold, formed from a 5 ns pulse of cold electrons. Main image is logarithmically scaled, inset is linearly scaled.

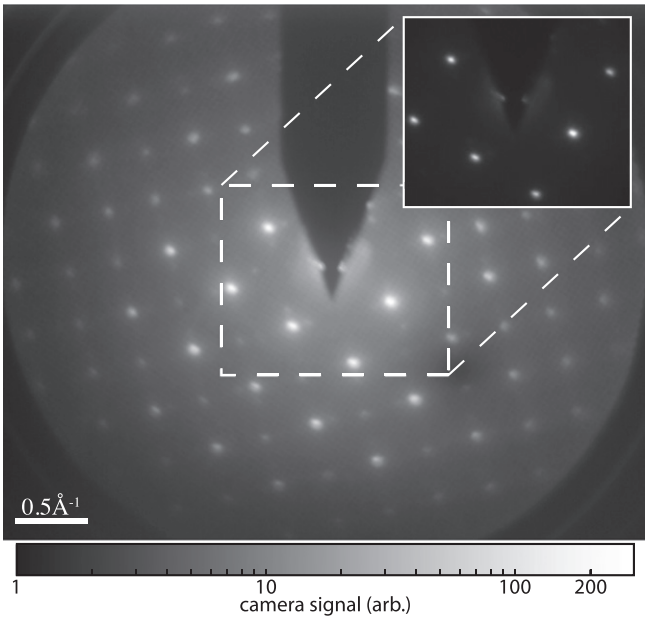

Figure 3. Two thousand diffraction shots from gold, directly averaged. Averaging results in a higher signal-to-noise ratio, but shot-to-shot beam instabilities lead to a broadening of the Bragg peaks. Main image is logarithmically scaled, inset is linearly scaled.

The reflections show the four-fold symmetry of the gold face-centered cubic (fcc) lattice, and the {200} and {220} reflections visible on the sides and corners of the inner square confirm the unit cell parameter as 0.407 nm, consistent with the accepted value for gold of 0.40782 nm at 25 °C [27]. To obtain a higher signal-to-noise ratio, 2000 shots were averaged. The result (figure 3) allows Bragg spots to be identified out to the $(\overline{6}60)$ reflection, with an effective resolution of 2.08 Å^{-1}, limited by the size of the detector.

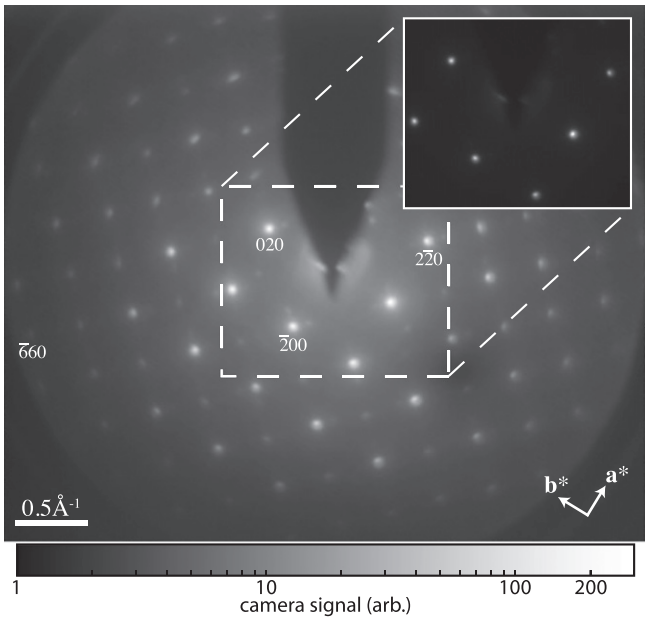

Figure 4. Two thousand diffraction shots from gold averaged by registering individual images. Registration is possible due to the high signal-to-noise ratio in the single shots, and recovers the sharpness in Bragg peaks lost in direct averaging. The reciprocal lattice vectors **a***, **b*** are drawn to scale. Main image is logarithmically scaled, inset is linearly scaled.

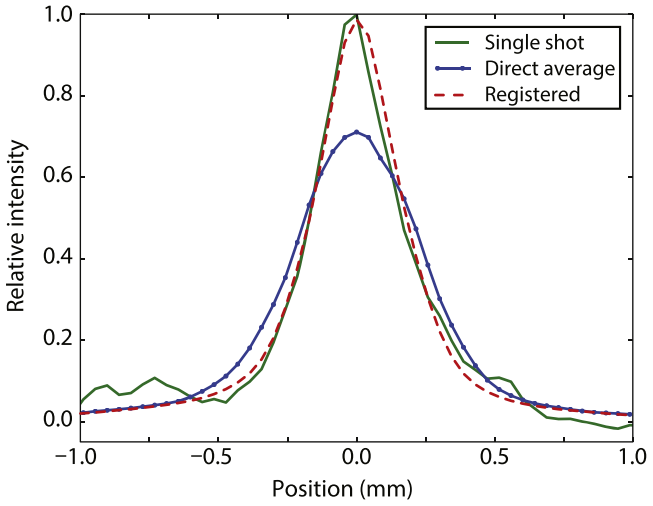

Figure 5. A lineout of the ($\bar{2}00$) Bragg reflection in the **b*** direction. Registering the single shots averages out the noise without resulting in Bragg spot broadening, as happens when shots are directly averaged.

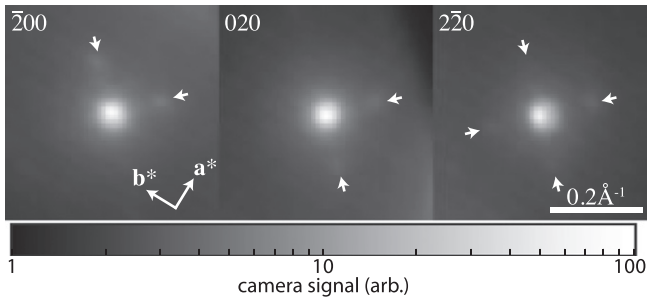

Figure 6. The two satellite spots around the ($\bar{2}00$) and (020) reflections, and the rightmost spot around the ($2\bar{2}0$) reflection, are due to diffraction from crystal twins. The other spots visible around the ($2\bar{2}0$) reflection are due to the electron diffracting twice: once each from two different twins. The small arrows indicate the positions of the faint satellite spots. The reciprocal lattice vectors are not to scale.

Closer inspection reveals that the Bragg spots have been significantly broadened when compared to the single-shot case, indicating that the transverse coherence of the time-averaged electron beam is reduced compared to any single constituent bunch. This loss of coherence stems from variation in the bunch trajectory related to small variations in the remnant magnetic field of the magneto-optic trap. The effect of the beam drift on the diffraction pattern is analogous to the varying shot-to-shot diffraction patterns obtained in XFEL nanocrystal diffraction experiments, where diffraction patterns are obtained from millions of randomly aligned nanocrystals [28].

To compensate for the beam wobble, successive single-shot images were registered. The eleven brightest spots were used to adjust the alignment by performing a cross correlation of the individual images and the unregistered average in the region surrounding the spots. The resulting registered average can be seen in figure 4, showing notably sharper Bragg spots.

A lineout (figure 5) of the ($\bar{2}00$) Bragg reflection in the **b*** direction shows how the direct average reduces the noise level compared to a single shot, at the expense of increasing peak width. The registered average maintains the low noise level of the direct average, while fully recovering the peak resolution. These results emphasize that the imaging is indeed effectively single-shot, with features clearly visible above the noise out to a resolution to 1.1 Å^{-1}.

Due to the structure amplitude of fcc gold, the only allowed reflections are those where the Miller indices h, k, l, are all even or all odd. The diffraction images of gold were taken along the $\langle 001 \rangle$ zone axis, where the lattice amplitude dictates that reflections are only allowed if h and k are even. While at low diffraction angles these rules are obeyed, it can be seen in figures 3 and 4 that some kinematically disallowed reflections are visible at higher angles. This is caused by a departure from the single scattering kinematic approximation, where both elastically, and inelastically scattered electrons are then re-scattered into directions which are forbidden to the unscattered incident beam. It can also be seen from figure 6 that the Bragg reflections are accompanied by two or more satellites, offset from the main reflection at 45° from the direction of the reciprocal basis vectors.

These satellites are the result of {111} crystal twinning, which can form when (100) gold films are prepared by evaporation [29]. There are two different mechanisms behind the satellite creation. The two relatively strong satellites that can be seen around the ($\bar{2}00$) and (020) Bragg reflections are created directly by diffraction from the crystal twins. This also produces the rightmost spot around the ($2\bar{2}0$) reflection. The other satellites around the ($2\bar{2}0$) reflection arise from double diffraction, where electrons are first diffracted by a

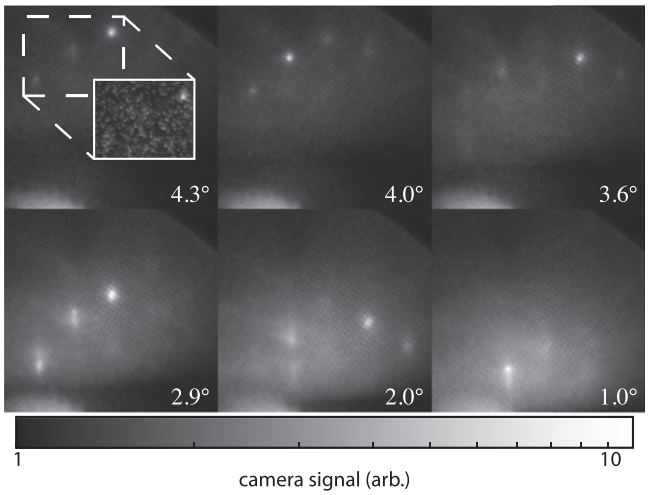

Figure 7. One hundred shot averages of RHEED from silicon ⟨100⟩ at a range of polar angles. Inset: a single shot of the region indicated, clearly showing a Bragg reflection.

(100) oriented domain, and then diffracted again by one of the twins. Dynamical effects would not normally be seen with such a thin sample because electron energies used in a transmission electron microscope are typically ten times greater than used here, resulting in a much lower scattering cross section and interactions that more closely match simple kinematic theory.

RHEED is a surface-sensitive diffraction technique routinely used to monitor crystal surface quality and epitaxial crystal growth [30], and has also been used to observe surface dynamics resulting from illumination by ultrafast lasers [31]. RHEED is a useful technique to further demonstrate diffraction from our source, both because the electron energies typically required are readily accessible, and because high quality single crystals are more readily available as bulk wafers than as the nanometre-thick foils needed for transmission electron diffraction. To adjust the system for RHEED required simple rotation of the sample by 90° as shown in figure 1(b)(ii). Figure 7 shows RHEED patterns from a ⟨100⟩ silicon wafer, which was HF etched to remove the native oxide layer immediately prior to transfer to the vacuum chamber. The beam was nominally incident on the crystal from the (110) direction at 0° polar angle. Since the sample stage could not be rotated in the azimuthal direction, it is likely that the wafer was slightly misaligned, which would account for the apparent horizontal asymmetry of the Bragg reflections at any particular polar angle. For clarity the RHEED patterns shown are 100 shot averages, however Bragg reflections were easily visible from a single shot as shown by the inset.

Cold electron RHEED offers a promising opportunity to investigate near-surface dynamics on nanosecond time scales. The high transverse coherence of the beam should also allow coherent scattering to be observed from structures tens of nanometres wide, such as quantum dots and optical metamaterials. Cold electron sources with bunch shaping to control space-charge induced brightness degradation are perhaps uniquely placed to perform these studies, due to their potential to deliver high bunch charges and high coherence at relatively low electron energies. Using very high electron energies to mitigate space-charge effects is not an option for RHEED, since very energetic electrons penetrate too deeply to accurately probe surface structure.

5. Summary

We have demonstrated single-shot electron diffraction using fast electron bunches produced with a CAES. The 5 ns bunches contained around 5×10^5 electrons, and because of their low temperature and high coherence, no beam aperture was required, allowing all generated electrons to contribute to imaging. When scattered by a single crystal of gold, the resulting single-shot diffraction pattern contained sufficient signal to give information about the crystal structure without averaging. The large signal-to-noise ratio allowed subsequent shots to be merged through image registration, which compensated for shot-to-shot beam drift that degraded the image quality when directly summing. Single-shot diffraction pattens have also been obtained in reflection mode, which may prove useful for investigating the dynamics of nanometre scale surface structures, where high beam coherence is necessary. Demonstrating single-shot diffraction is a significant step forward for CAESs, and supports the promise that they could complement solid state photocathode sources for use in ultrafast single-shot electron diffraction experiments.

Acknowledgments

We thank L J Allen for helpful discussions and advice. BMS gratefully acknowledges the support of a University of Melbourne McKenzie Fellowship. This work was supported by the Australian Research Council Discovery Project DP140102102.

References

[1] Barty A *et al* 2008 *Nat. Photonics* **2** 415–9
[2] Dwyer J R, Hebeisen C T, Ernstorfer R, Harb M, Deyirmenjian V B, Jordan R E and Miller R J D 2006 *Phil. Trans. R. Soc.* A **364** 741–78
[3] Zewail A H 2006 *Annu. Rev. Phys. Chem.* **57** 65–103
[4] Seibert M M *et al* 2011 *Nature* **470** 78–81
[5] Chapman H N *et al* 2006 *Nat. Phys.* **2** 839–42
[6] Neutze R, Wouts R, van der Spoel D, Weckert E and Hajdu J 2000 *Nature* **406** 752–7
[7] Quiney H M and Nugent K A 2011 *Nat. Phys.* **7** 142–6
[8] Carbone F, Musumeci P, Luiten O and Hebert C 2012 *Chem. Phys.* **392** 1–9
[9] Henderson R 1995 *Q. Rev. Biophys.* **28** 171–93
[10] Krivanek O and Mooney P 1993 *Ultramicroscopy* **49** 95–108
[11] van Oudheusden T, Pasmans P L E M, van der Geer S B, de Loos M J, van der Wiel M J and Luiten O J 2010 *Phys. Rev. Lett.* **105** 264801

[12] Claessens B J, van der Geer S B, Taban G, Vredenbregt E J D and Luiten O J 2005 *Phys. Rev. Lett.* **95** 164801
[13] Tokita S, Inoue S, Masuno S, Hashida M and Sakabe S 2009 *Appl. Phys. Lett.* **95** 111911
[14] Li R *et al* 2010 *Rev. Sci. Instrum.* **81** 036110
[15] Musumeci P, Moody J T, Scoby C M, Gutierrez M S, Bender H A and Wilcox N S 2010 *Rev. Sci. Instrum.* **81** 013306
[16] Sciaini G, Harb M, Kruglik S G, Payer T, Hebeisen C T, Heringdorf F J M z, Yamaguchi M, Hoegen M H v, Ernstorfer R and Miller R J D 2009 *Nature* **458** 56–59
[17] Siwick B J, Dwyer J R, Jordan R E and Miller R J D 2003 *Science* **302** 1382–5
[18] McCulloch A J, Sheludko D V, Junker M and Scholten R E 2013 *Nat. Commun.* **4** 1692
[19] Engelen W J, van der Heijden M A, Bakker D J, Vredenbregt E J D and Luiten O J 2013 *Nat. Commun.* **4** 1693
[20] McCulloch A J, Sheludko D V, Saliba S D, Bell S C, Junker M, Nugent K A and Scholten R E 2011 *Nat. Phys.* **7** 785–8
[21] Luiten O J, van der Geer S B, de Loos M J, Kiewiet F B and van der Wiel M J 2004 *Phys. Rev. Lett.* **93** 094802
[22] van Mourik M W, Engelen W J, Vredenbregt E J D and Luiten O J 2014 *Struct. Dyn.* **1** 034302
[23] Zurch M, Rothhardt J, Hadrich S, Demmler S, Krebs M, Limpert J, Tunnermann A, Guggenmos A, Kleineberg U and Spielmann C 2014 *Sci. Rep.* **4** 7356
[24] van Oudheusden T, de Jong E F, van der Geer S B, t Root W P E M O, Luiten O J and Siwick B J 2007 *J. Appl. Phys.* **102** 093501
[25] Egerton R F 2015 *Adv. Struct. Chem. Imaging* **1** 5
[26] Luiten O J, Claessens B J, van der Geer S B, Reijnders M P, Taban G and Vredenbregt E J D 2007 *Int. J. Mod. Phys.* A **22** 3882–97
[27] Maeland A and Flanagan T B 1964 *Can. J. Phys.* **42** 2364–6
[28] Chapman H N *et al* 2011 *Nature* **470** 73–77
[29] Pashley D W and Stowell M J 1963 *Phil. Mag.* **8** 1605–32
[30] Neave J, Joyce B, Dobson P and Norton N 1983 *Appl. Phys.* A **31** 1–8
[31] Elsayed-Ali H E and Herman J W 1990 *Appl. Phys. Lett.* **57** 1508–10